*Free Rad. Res. Comms.*, Vol. 15, No. 5, pp. 245–253
Reprints available directly from the publisher
Photocopying permitted by license only



# ONE- AND TWO-DIMENSIONAL ELECTRON PARAMAGNETIC RESONANCE IMAGING IN SKIN

JÜRGEN FUCHS‡, HANS JOACHIM FREISLEBEN§, NORBERT GROTH¶, THOMAS HERRLING¶, GUIDO ZIMMER§, RAINER MILBRADT and LESTER PACKER

*‡Zentrum der Dermatologie und Venerologie, Abteilung II, §Zentrum der Biologischen Chemie, Universitätsklinikum, Theodor Stern Kai 7, 6000 Frankfurt/M 70, and ¶Zentrum für Wissenschaftlichen Gerätebau, Akademie der Wissenschaften, Rudower Chaussee 6, Berlin 1199, Germany. Department of Molecular and Cell Biology, University of California Berkeley, Berkeley, CA 94720, USA*

*(Received February 4, 1991; in final form June 28 1991)*

EPR imaging with modulated field gradients provides the possibility for obtaining an EPR spectrum in a selected volume. We demonstrate the feasibility of X-band (9.5 GHz) electron paramagnetic resonance (EPR) imaging in skin biopsies of hairless mice. One- (1D) and two-dimensional (2D) EPR images of the persistent free radical di-tertiary-butyl-nitroxide are measured. At a microwave frequency of 9.5 GHz (X-band), 2D images are obtained in skin biopsies with an actual point distinction resolution of 25 $\mu$m. In a biological model system, 2D images are measured at L-band frequency (2.0 GHz) with a pixel resolution of 61 $\mu$m, and a theoretical spatial resolution of 12.5 $\mu$m. In combination with the spin labeling and spin trapping technique, EPR imaging is the most direct approach to analyzing spatial distribution of physicochemical properties in skin, such as membrane fluidity and polarity, as well as detection of free radicals.

KEY WORDS: EPR spectroscopy, EPR imaging, free radicals, nitroxides, skin.



## INTRODUCTION

Electron paramagnetic resonance (EPR) measurements allow chemical characterisation of a paramagnetic species in biological tissue and analysis of its physicochemical reactivity. EPR signals exist in normal tissues as a result of physiological processes. Intensity of these resonance signals is however usually low. Because of the weak signal intensity of natural radicals in tissues, paramagnetic spin labels are used in EPR spectroscopy. The basis of the labeling technique are compounds containing the paramagnetic nitroxide moiety. Nitroxides offer certain advantages in synthetic versatility, in sensitivity to motion, polarity, structural order and fluidity, oxygen tension, redox processes, and bioenergetic parameters. Therefore, nitroxide spin probes and their precursors (nitrones) are extensively used in molecular and cellular biology for purposes such as spin labeling, spin trapping (nitrones), oximetry, viscosimetry, redox probing of cellular environments, and bioenergetic measurements. Nitroxides are also used for spin labeling drugs, thus allowing detection of the labeled compound by means of EPR spectroscopy.

Magnetic resonance tomography involving both EPR and NMR (nuclear magnetic resonance) imaging are concerned with the spatial distribution of electron or nuclear spins in heterogenous samples. EPR imaging is a new and emerging technique dating back no more than two decades. The novel idea of imaging was suggested by Paul

Lauterbur in 1973,[1] which finally led to development of the NMR imaging technique. In unpublished EPR experiments Lauterbur also demonstrated the phenomenon of EPR imaging using a phantom probe. In the late 70's and early 80's Karthe,[2] Hoch,[3] Ohno,[4] and Lebedev,[5] independently published reports regarding EPR imaging applications to various solid state problems. In 1982 Herrling developed an EPR imaging method, using conventional X-band EPR spectroscopy combined with the modulated field gradient technique.[6] Field gradient EPR spectroscopy at X-band was used by Kristl to measure one-dimensional EPR images of spin probes (nitroxides) and spin labeled drugs in ointments.[7] Two-dimensional ENDOR images were obtained from phantom samples and plant stems containing nitroxides.[8] A compilation of current literature was given by Eaton.[9] In this paper we report a feasibility study of EPR imaging in skin. We have studied one- and two-dimensional EPR images of nitroxide spin probes in skin biopsies of hairless mice at X-band (9.5 GHz), and in a biological model system at L-band (2 GHz) frequency.

## MATERIALS AND METHODS

### *EPR Imaging*

The EPR 221 and the imaging unit ZZG1 were developed and built at the Zentrum für Wissenschaftlichen Gerätebau, Akademie der Wissenschaften, Berlin. For X-band (9.5 GHz) measurements a rectangular standard resonance cavity with a $H_{102}$ mode was used, for L-band (2 GHz) measurements a surface coil (7 mm diameter) was applied. The imaging unit consists of a gradient coil unit which is arranged between the pole pieces and the cavity. Both gradient coils and the amplifier are water cooled. A schematic outline of the EPR imaging system is presented in Figure 1. The magnet,

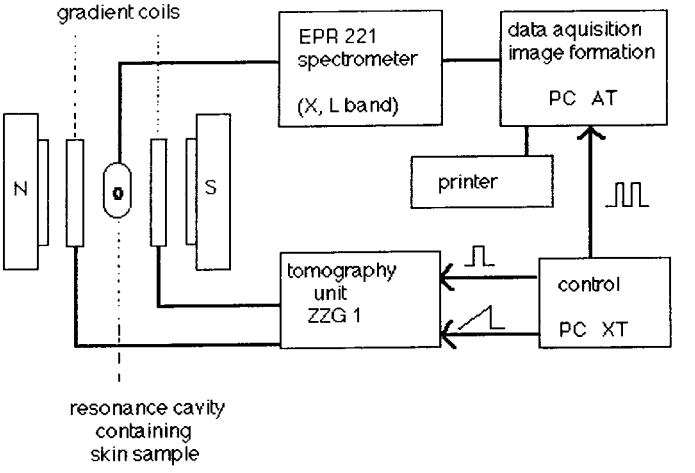


FIGURE 1 EPR imaging unit. The spectra were measured for 64 spatial planes with 64 points. Every spectrum was measured by 256 spectral points, which was interpolated for 64 points. The registration time for every spectrum and one-dimensional (1D) image was 2 sec, and 128 sec for a two-dimensional (2D) image. The spectral range for the fast scans was 6 mT.

gradient coils, microwave components, and detection device are described.[10] The instrument settings for X-band measurements are: Central magnetic field 339.0 mT, modulation frequency 50 kHz (second harmonic), modulation amplitude 0.2–0.35 mT, field gradient 4 T/m, microwave power 50 mW, continuous mode, gradient frequency 45 Hz. For L-band measurements the field gradient is 1 T/m.

### *Animals and Chemicals*

Euthymic, hairless female-mice [SKH1 (hr/hr) Br], were purchased from Charles River Wiga GmbH, Sulzfeld, FRG, and fed with a standard diet. 6 mm punch biopsies were cut from the animals, and skin thickness was determined with a spring loaded caliper gauche. Di-tertiary-butyl-nitroxide (DTBN), and dimethylsulfoxide (DMSO) were purchased from Sigma, München, FRG.

## RESULTS

### *X-band: Spatial 1D Image*

Time dependent penetration of the lipophilic spin label di-tertiary-butyl-nitroxide (DTBN) is measured in gelatine (Figure 2), and in skin biopsies of hairless mice in absence (Figure 3), or presence of the penetration enhancer DMSO (Figure 4). Repetitive scans of the 1D spatial distribution of DTBN are shown. The left resonance

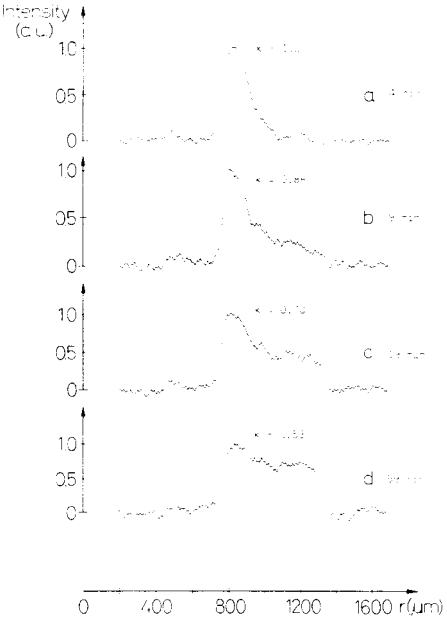


FIGURES 2–4 X-band imaging in model systems. A quartz tissue cell with a central hole (0.5 mm deep, 4 mm in diameter) is filled with gelatine (Figure 2). A spin label solution (DTBN 50 mM in Polysorbat 80, a viscous sorbitan-fatty acid ether/ester) is placed in a reservoir chamber (0.2 mm deep, 4 mm in diameter) on top of the gelatine or on the epidermal side of a skin biopsy fixed in the tissue cell (Figures 3 and 4). In Figure 4 DMSO is added to the spin label solution at a final concentration of 10%. Repetitive spatial 1D images are shown.

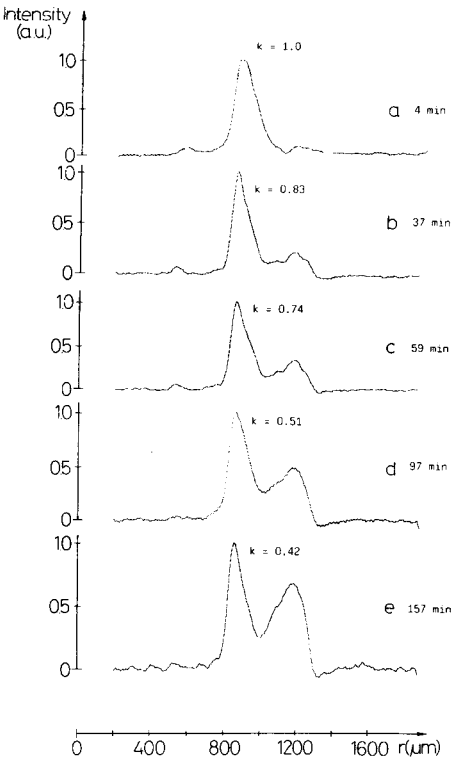


FIGURE 3

peak represents the nitroxide reservoir at the sample surface. The right resonance peak, which slowly increases over time, is assigned to DTBN penetrating and accumulating in the gelatine or skin biopsy. The signal amplitude corresponds to the nitroxide concentration, signal loss during the experiment is due to nitroxide reduction in skin. The 1D images are normalized to a signal maximum [arbitrary units (au)]. Absolute signal intensities are given by a factor ($k$). DMSO enhances penetration several-fold, a concentration equilibrium is already reached after 59 min (Figure 4d versus Figure 3c). DMSO also facilitates reduction of the spin label as indicated by a rapid decrease of absolute signal intensity.

### *X-band: Spectral–Spatial 2D Image*

A two-dimensional (2D) image of DTBN penetrating into skin is shown in Figure 5a, 15 min after administration of the spin label at the epidermal surface. Signal intensity is displayed on the $z$-axis, magnetic field [$B$ (mT)] on the $x$-axis, and skin thickness [$r$ ($\mu$m)] on the $y$-axis. Total skin thickness was about 800 $\mu$m and epidermal thickness 60 $\mu$m as shown by light microscopy. With a 2D image matrix of 64 $\times$ 64 pixels the pixel resolution in Figure 5a is 12.5 $\mu$m. However the actual point distinction resolution is 25 $\mu$m. A grey scale distribution of the 2D image is shown in Figure 5b, as

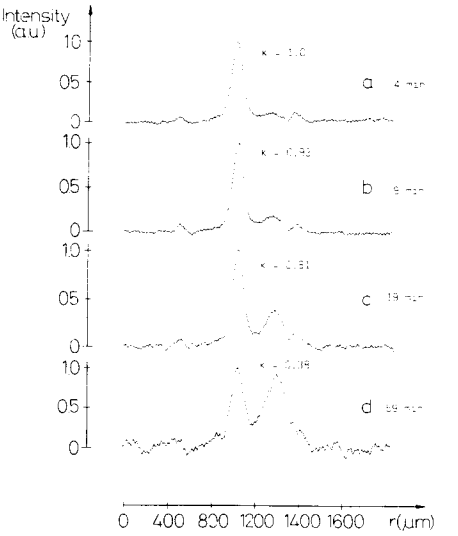


FIGURE 4

viewed from the perspective perpendicular to the $x$–$y$ plane. In Figure 5c an EPR spectrum (2nd. harmonic) recorded in the epidermal plane is shown. The 2D image displayed in Figure 5d (45 min) shows time dependent skin penetration of DTBN, and a significant loss of signal intensity, which is due to spin label reduction.

*L-Band: Spatial 2D Image*

L-band imaging was performed by surface coil measurements. A plant stem is chosen as a biological model system to study resolution of L-band imaging for the following reasons. (1) The presence of a defined vascular system (phloem and xylem) inside the stem allows spatial analysis of heterogenous nitroxide distribution. (2) Due to the limited thickness of hairless mouse skin (800 $\mu$m maximal skin thickness), analysis of the spatial resolution of the deeper penetrating L band microwaves requires thicker samples. In Figure 6 the 2D spatial–spatial image of DTBN distribution in the stem of Dieffenbachia picta is shown. The plant parenchyma and vascular system can be distinguished by different grey scale intensity. The total diameter of the plant stem is 5 mm, the pixel resolution is 61 $\mu$m.

## DISCUSSION

*X-Band 1D and 2D Imaging*

1D spatial imaging provides rapid information about liberation, penetration and accumulation of a paramagnetic compound in skin. The fast scan technique allows

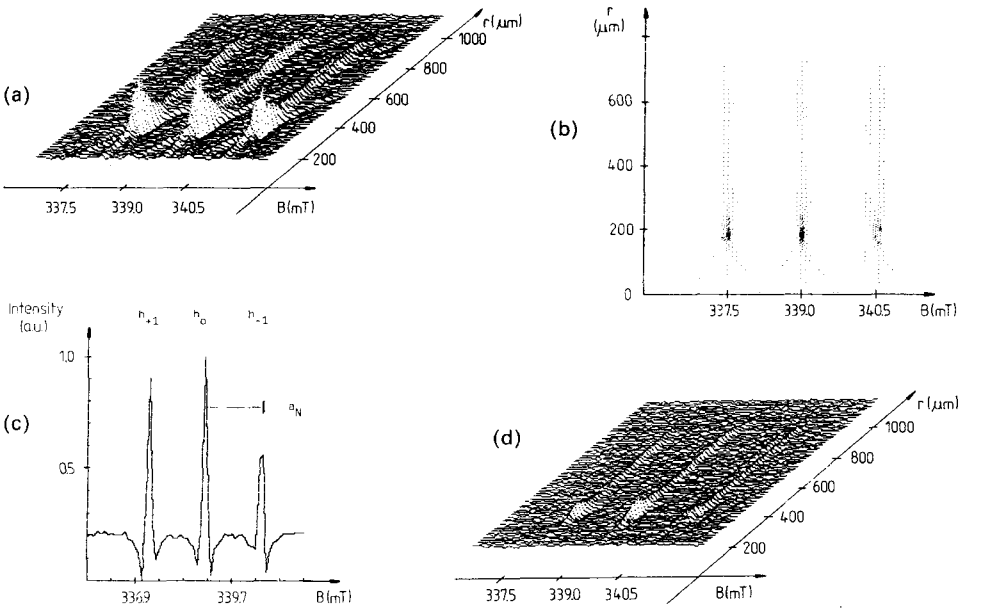


FIGURE 5 X-band imaging in skin. A spin label solution of DTBN 50 mM in ethanol/water (50/50) is placed on the epidermal surface of a freshly excised skin biopsy. Penetration of the spin label into epidermis and dermis is measured by repetitive scans. (a) Shows the spectral–spatial 2D image after 15 min, in (b) a grey scale distribution pattern is displayed, and in (c) the EPR spectrum (2nd harmonic) in the epidermis is shown. (d) Displays the 2D image after 45 min.

rapid data accumulation and this approach is particularly suited for measurement of fast penetration kinetics. 1D skin imaging can easily be used for visualizing the penetration enhancement effect of DMSO. Accumulation time of 2D images (128 sec) is 64 fold slower than that of 1D images (2 sec), therefore rapid penetration processes on the time scale of a few seconds up to a few minutes cannot be analyzed by 2D imaging.

DTBN penetrates more rapidly into gelatine than into mouse skin (Figure 2d versus Figure 3c). In comparison to skin biopsies, a different penetration profile (spatial 1D image) of DTBN is obtained in gelatine. This is presumably due to compartimentation of skin into morphologically and biochemically distinct layers, exhibiting different polarities and metabolic activities. In gelatine and skin biopsies there is significant reduction of the resonance signal intensity (decrease of the $k$ factor), due to spin label reduction into EPR silent products.[11]

2D spectral–spatial images provide more detailed information than 1D spatial images, e.g. they allow measurement of an EPR spectrum in a selected tissue plane and analysis of spectral changes. The increase of the $h_0/h_{-1}$ ratio in epidermis spin labeled with DTBN (Figure 5c), in comparison to the ratio of DTBN in water (not shown), indicates immobilisation of the spin label in skin. The $a_N$ value can give an indication of the medium polarity and may be used for measurement of skin hydration.

*Spatial Resolution of EPR Imaging*

The actual point distinction resolution $dR$ is determined by the ratio of the spectral line width of the paramagnetic center $dB_{1/2}$ and the field gradient $grdB$, multiplied with

a factor $f$ [$dR = (dB_{1/2}/grdB) \times f$]. The factor $f$ is determined by (1) the modulation function of the field gradient, (2) the spectral line shape function, (3) the resolution criterion, and (4) the derivative of the spectrum. In addition, the signal to noise ratio of the intrinsic measurement is a critical factor. Corresponding to the method suggested by Sparrow (described by Janson) for determination of the actual spatial resolution of two equal paramagnetic centers characterized by a Lorentz curve (2nd harmonic),[12] the factor $f$ for a cosinus modulation is $f = 0.38$ ($f = 0.5$ for a triangular modulation). For a spectral line width of 0.1 mT, a field gradient of 5 T/m a theoretical resolution (actual point distinction) of 7 $\mu$m can be achieved for X- and L-band measurements. The pixel resolution $dR_{pix}$, which depends on the reconstruction software, is determined by the ratio of the image size (sample thickness) $I_p$ and the number of pixels measured $n_{pr}$ [$dR_{pix} = I_p/n_{pr}$]. In Figure 5a the spectral line width is 0.2 mT, field gradient 4 T/m, and $f = 0.5$ (triangular modulation). Therefore the actual point distinction resolution $dR$ is 25 $\mu$m. However, the pixel resolution $dR_{pix}$ in Figure 5a is 12.5 $\mu$m (sample thickness 800 $\mu$m, 64 spatial planes).

Surface coil measurements in the plant stem reveal a spatial 2D image of nitroxide distribution, visualizing plant parenchyma and vascular system. At a microwave frequency of 2 GHz, biological samples of 5 mm thickness can easily be imaged. Although the theoretical spatial resolution at L-band frequency is similar to that of X-band frequency (7 $\mu$m), the point to point resolution of the L-band experiment in Figure 6 is only 61 $\mu$m (12.5 $\mu$m for X-band). To achieve the actual point distinction resolution of 12.5 $\mu$m, a pixel matrix of 512 $\times$ 512 (instead of 64 $\times$ 64) would be required. Due to lower sensitivity at L-band frequency, data aquisition time (scan time) was 8.4 fold of that used for the X-band measurement.

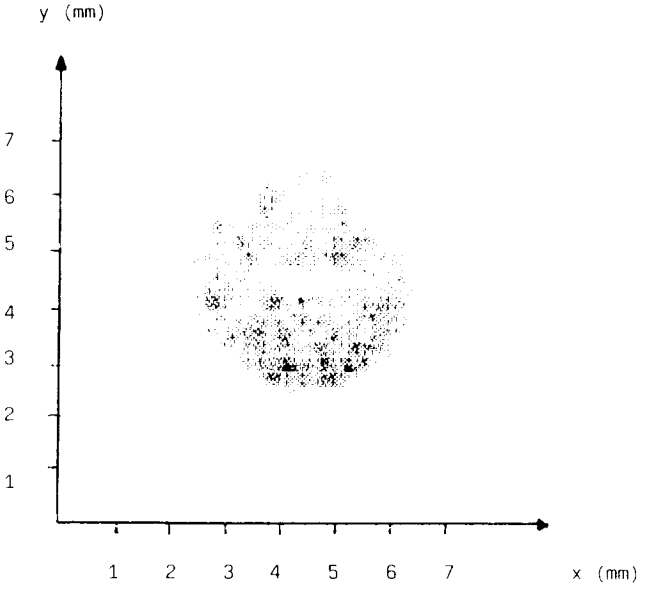


FIGURE 6 L-band imaging in a biological model. A spatial 2D image of a Dieffenbachia picta stem is shown. The plant stem is placed vertically in a 50 mM solution (water) of DTBN for 30 min. Subsequently the image is recorded with a scan time of 18 min.

### *Microwave Tissue Penetration*

Tissue penetration of microwaves varies considerably with the tissue investigated and is mainly a function of tissue water content. In muscle tissue (water content 76–80%) X-band (9 GHz) microwaves penetrate about 1.5 mm, and in fat tissue (water content 10–30%) about 25 mm. L-band (1 GHz) microwaves penetrate about 18 mm into muscle, and 70 mm into fat tissue.[13–15] The skin is not an organ particularly rich in water, it has the lowest amount of water per unit weight among soft tissues. The water content of rodent and human epidermis is in the same range as that of total skin (65–70%), however the horny layer is extremely poor in water (10–30%). It is extrapolated from these data that X-band and L-band frequency can be used for imaging skin specimens having a total thickness of 3.5 mm, and 35 mm, respectively. This indicates that EPR imaging at X- and L-band frequency can be used for imaging skin and subcutaneous structures.

### *Conclusion*

EPR spectroscopy is of increasing importance in dermatologic research. It has been applied for studying skin membrane fluidity and polarity,[16–20] oxygen diffusion in skin,[21] detection of highly reactive free radicals by spin trapping,[22–23] and direct detection of persistent free radicals.[24–26] EPR imaging allows spatial analysis of all these processes and can be used for "biophysical and biochemical skin microscopy" *in-vitro* as well as *in-vivo* (applying surface coils). The major difficulty with conventional X-band (9.5 GHz) EPR instrumentation for biological samples is the high dielectric absorbtion brought about by the presence of water and ions. An important methodological break through is accomplished by using low microwave frequencies (L-band, 1–2 GHz), thereby significantly reducing microwave absorption for biological materials. The increase in microwave tissue penetration is however accompanied by a loss in sensitivity. X-band frequency has severe technical limitations for most *in-vivo* EPR imaging studies. However, we demonstrate that it is especially suited for skin imaging. X-band microwaves penetrate about 3.5 mm into skin. Surface coil measurements at L-band frequency, with microwaves penetrating at least 35 mm into skin, allow EPR imaging of subcutaneous structures.

### *References*

1. P.C. Lauterbur (1973) Image formation for induced local interactions: examples employing nuclear magnetic resonance. *Nature*, **242**, 190–191.
2. W. Karthe and E. Wehrsdorfer (1979) The measurement of inhomogenous distributions of paramagnetic centers by means of EPR. *Journal of Magnetic Resonance*, **33**, 107–111.
3. M.J.R. Hoch and A.R. Day (1979) Imaging of paramagnetic centers in diamond. *Solid State Communications*, **30**, 211–213.
4. K. Ohno (1981) A method of EPR imaging: application to spatial distributions of hydrogen atoms trapped in sulfuric acid ices. *Japanese Journal of Applied Physics*, **20**, 179–182.
5. E.Y. Galtseva, O.Y. Yakimchenko and Y.S. Lebedev (1983) Diffusion of free radicals as studied by tomography. *Chemical Physics Letters*, **99**, 301–304.
6. T. Herrling, N. Klimes, W. Karthe, U. Ewert and B. Ewert (1982) EPR zeugmatography using modulated magnetic field gradients. *Journal of Magnetic Resonance*, **49**, 203–211.
7. J. Kristel, S. Pecar, J. Korbar-Smid, F. Demsar and S. Schara (1989) Drug diffusion: a field gradient electron paramagnetic resonance study. *Drug Development and Industrial Pharmacy*, **15**, 1423–1440.
8. Y. Kotake, U.M. Oehler and E.G. Janzen (1988) Two-dimensional ENDOR imaging based on differences in oxygen concentration. *Journal Chemical Society Faraday Transaction*, **84**, 3275–3278.

9. G.R. Eaton and E.E. Eaton (1988) EPR imaging: progress and prospects. *Bulletin of Magnetic Resonance*, **10**, 22–31.
10. T. Herrling (1991) Modulated field gradient: instrumentation. In *EPR imaging and in-vivo EPR* (G.R. Eaton, E.E. Eaton & K. Ohno, eds.), CRC Press, in press.
11. J. Fuchs, R.J. Mehlhorn and L. Packer (1989) Free radical reduction mechanisms in mouse epidermis and skin homogenates. *Journal of Investigative Dermatology*, **93**, 633–640.
12. P.A. Janson (1984) *Deconvolution with application in spectroscopy*. Academic Press, London.
13. J. Bernhardt (1979) Biologische Wirkung elektromagnetischer Felder. *Zeitschrift für Naturforschung*, **34c**, 616–627.
14. A.Y. Cheung, W.M. Golding and G.M. Samaras (1981) Direct contact applications for microwave hyperthermia. *Journal of Microwave Power*, **16**, 151–159.
15. D.V. Land (1986) Microwave thermographic technique for clinical medical applications. In *Colloquium on "Industrial and Medical Applications of Microwaves"*, Digest No. 1986/73, Institution of Electrical Engineers, Savoy Place, London, WC2R 0BL.
16. S.J. Rehfeld, W.Z. Plachy, E.S. Hou and P.M. Elias (1989) Localization of lipid phase transitions in hairless mouse stratum corneum by electron spin resonance. *Journal of Investigative Dermatology*, **92**, 505.
17. S.J. Rehfeld, W.Z. Plachy, M.L. Williams and P.M. Elias (1988) Calorimetric and electron spin resonance examination of lipid phase transitions in human stratum corneum: molecular basis for normal cohesion and abnormal desquamation in recessive X-linked ichthyosis. *Journal of Investigative Dermatology*, **91**, 499–505.
18. T. Tanaka, T. Hidaka, R. Ogura and M. Sugiyama (1988) Changes of membrane fluidity and $Na^+$, $K^+$ ATPase activity during cellular differentiation in the guinea pig epidermis. *Archives of Dermatologic Research*, **280**, 29–32.
19. T. Tanaka, R. Ogura, T. Hidaka and M. Sugiyama (1989) Changes of electron spin resonance membrane fluidity in hexadecane induced hyperproliferative epidermis. *Journal of Investigative Dermatology*, **93**, 682–686.
20. T. Tanaka, T. Sakanashi, N. Kaneko and R. Ogura (1989) Spin labeling study on membrane fluidity of epidermal cell (cow snout epidermis). *Journal of Investigative Dermatology*, **87**, 745–747.
21. W.Z. Plachy and M.E. Hatcher (1990) Dioxygen diffusion in the stratum corneum. *Journal of Investigative Dermatology*, **94**, 567.
22. J. Schreiber, G.L. Foureman, M.F. Hughes, R.P. Mason and T.E. Eling (1989) Detection of glutathione thiyl free radical catalyzed by prostaglandin H synthase present in keratinocytes. *Journal of Biological Chemistry*, **264**, 7936–7943.
23. B.G. Taffe, N. Takahashi, T.W. Kensler and R.P. Mason (1987) Generation of free radicals from organic hydroperoxide tumor promoters in isolated mouse keratinocytes. *Journal of Biological Chemistry*, **262**, 12143–12149.
24. J. Fuchs and L. Packer (1989) Investigations on anthralin free radicals in model systems and in skin of hairless mice. *Journal of Investigative Dermatology*, **92**, 677–682.
25. P.A. Riley (1970) Mechanism of pigment cell toxicity produced by hydroxyanisole. *Journal of Pathology*, **101**, 163–169.
26. B. Schroot and C. Brown (1986) Free radicals in skin exposed to dithranol and its derivatives. *Arzneimittel Forschung/Drug Research*, **36**, 1253–1255.

Accepted by Prof. H. Sies